Synergistic Activity of Floor-Plate- and Ventricular-Zone-Derived Netrin-1 in Spinal Cord Commissural Axon Guidance

Juan Antonio Moreno-Bravo, Sergi Roig Puiggros, Patrick Mehlen, Alain Chédotal

HAL Id: hal-02340095

https://hal.sorbonne-universite.fr/hal-02340095

Submitted on 30 Oct 2019

Synergistic activity of floor plate and ventricular zone-derived netrin-1 in spinal cord commissural axon guidance

Juan Antonio Moreno-Bravo[1,†], Sergi Roig Puiggros[1,†], Patrick Mehlen[2] and Alain Chédotal [1, 3, *]

[1] Sorbonne Université, INSERM, CNRS, Institut de la Vision, 17 Rue Moreau, F-75012 Paris, France.

[2] Apoptosis, Cancer and Development Laboratory, Equipe labellisée 'La Ligue', LabEx DEVweCAN, Centre de Recherche en Cancérologie de Lyon, INSERM U1052-CNRS UMR5286, Université de Lyon, Centre Léon Bérard, 69008 Lyon, France.

[3] lead contact

† These authors contributed equally

*Corresponding author: alain.chedotal@inserm.fr

Summary

In vertebrates, commissural axons extend ventrally toward the floor plate in the spinal cord and hindbrain. Netrin-1, secreted by floor plate cells, was proposed to attract commissural axons at a distance. However, recent genetic studies in mice have shown that netrin-1 is also produced by ventricular zone (VZ) progenitors and that in the hindbrain, it represents the main source of netrin-1 for commissural axons. Here we show that genetically deleting netrin-1 either from the VZ or the floor plate does not prevent midline crossing in the spinal cord although axon pathfinding and fasciculation are perturbed. Strikingly, VZ and floor plate act synergistically as the simultaneous ablation of netrin-1 from these two sources severely impede crossing. These results suggest that floor plate-derived netrin-1 has distinct impact on commissural axons in the spinal cord and the hindbrain.

Keywords: Netrin, spinal cord, axon guidance, floor plate, Dcc, commissure, motor neurons, ventricular zone, mouse

Introduction

In the central nervous system (CNS) of bilaterally symmetric animals, commissural neurons project their axons to the contralateral side (Chédotal, 2014). In vertebrates, most commissural axons grow ventrally and cross the midline at the level of the floor plate in the midbrain, ventral hindbrain and spinal cord (SC). Understanding the cellular and molecular mechanisms guiding commissural axons toward the ventral midline has been a central question in developmental neurobiology (Chédotal, 2011; Goodman, 1996). At the end of the XIXth century, Ramón y Cajal proposed that floor plate cells secrete chemoattractants for commissural axons (Ramón y Cajal, 1892). The first evidence supporting this hypothesis came about a century later using *in vitro* explant assays (Tessier-Lavigne et al., 1988). Thus far, three floor plate-derived chemoattractive factors were identified, netrin-1 (Kennedy et al., 1994; Serafini et al., 1994), Sonic hedgehog (Shh)(Charron et al., 2003) and vascular endothelial growth factor (VEGF)(Ruiz de Almodovar et al., 2011). All attract commissural axons *in vitro* and induce growth cone turning, but netrin-1 also has growth-promoting activity. Knockout mice lacking their respective receptors, Deleted in colorectal cancer (Dcc), Brother of CDO (Boc) or Fetal liver kinase 1 (Flk1) exhibit commissural axon guidance defects. In *Boc* and *Flk1* mutant embryos, commissural axons invade the motor columns and defasciculate in the ventral SC; however, midline crossing appears unaffected (Okada et al., 2006; Ruiz de Almodovar et al., 2011). By contrast, midline crossing is strongly impaired in the SC of mice lacking Dcc (Fazeli et al., 1997) and almost abrogated when the neogenin receptor is simultaneously inactivated (Xu et al., 2014). This is also the case in netrin-1 null and hypomorphic mutant mice (Bin et al., 2015; Dominici et al., 2017; Serafini et al., 1996; Yung et al., 2015). Therefore, netrin-1 is essential for commissural axon guidance in the SC. In

the hindbrain and SC, netrin-1 is not only present in floor plate cells but also in the ventral two thirds of the ventricular zone (VZ) (Dominici et al., 2017; Kennedy et al., 1994, 2006; Varadarajan et al., 2017). Surprisingly, recent studies using netrin-1 conditional mice, showed that the VZ is the major source of netrin-1 for hindbrain commissural axons, both promoting their ventral growth and preventing them from exiting the central nervous system (Dominici et al., 2017; Moreno-Bravo et al., 2018; Yamauchi et al., 2017; Yung et al., 2018). By contrast, no midline crossing defects were detected in the hindbrain following netrin-1 deletion from floor plate (Dominici et al., 2017). The partial deletion of netrin-1 from the SC VZ also results in axon guidance errors, but to a much lesser extent than in the hindbrain (Varadarajan et al., 2017). Following netrin-1 deletion from the floor plate in the SC many axons reached the midline normally, although a detailed analysis of trajectories and crossing was not conducted (Dominici et al., 2017; Varadarajan et al., 2017). These unexpected results questioned the role of netrin-1 at the floor plate. Given the high expression of netrin-1 at the midline, does it really play no role in guidance to and across the midline? Here we report that, in fact, netrin-1 from the floor plate and from the VZ do each individually contribute to commissural axon guidance in the SC, and that these two netrin-1 sources act synergistically to guide commissural axons as only the simultaneous deletion of netrin-1 from the VZ and floor plate leads to an almost complete lack of midline crossing. These results suggest that the function of floor plate netrin-1 might differ between the SC and the hindbrain.

Results

The ablation of netrin-1 from the VZ, using a *Nestin1:cre* (*Nes:cre*) line severely compromises midline crossing in the hindbrain (Dominici et al., 2017; Yamauchi et

al., 2017). Similar experiments in the SC (Varadarajan et al., 2017) showed that a partial deletion of VZ-netrin-1 is accompanied by the abnormal projection of commissural axons into the VZ, but midline crossing still occurs. These results suggested that the contribution of VZ-netrin-1 could differ between the hindbrain and SC or that there was still enough VZ-netrin-1 to guide axons ventrally. To address this question, we first compared the expression pattern of *netrin-1* mRNA of wild type and *Nes:cre;Ntn1fl/fl* embryos between E9 and E11 (Figures S1A-S1C and S1E-S1G). This showed that at E9, *Ntn1* levels in the VZ and floor plate appeared comparable in control (n=5) and *Nes:cre;Ntn1fl/fl* embryos (Figures S1A and S1E; n=3). However, at E10 (n=3), *Ntn1* level was reduced in the ventral SC VZ in *Nes:cre;Ntn1fl/fl* embryos and by E11 (n=5), it only remained detectable in the floor plate (Figures S1B-S1C and S1F-S1G). Accordingly, in *Nes:cre;RosaTom* embryos (n=9 embryos, 3 for each stage), tdTomato was only present in a few cells at E9, in a mosaic of VZ cells and motor neurons at E10, but covered the entire SC (except the floor plate) at E11 (Figures S1I-S1M). This shows that the slow onset of cre recombinase activity in the SC of *Nes:cre;Ntn1fl/fl* embryos only partially removed *Ntn1* from SC VZ at early developmental stages, coinciding with the appearance of the first commissural neurons (Dominici et al., 2017). We next studied the distribution of netrin-1 protein at E11 (n=5 for each genotype) and confirmed that in wild type SC (Figure S1D), netrin-1 was present on commissural axons, floor plate, the pial surface and processes of VZ progenitors (Dominici et al., 2017; Varadarajan et al., 2017). In *Nes:cre;Ntn1fl/fl* embryos, netrin-1 was absent from the pial surface and VZ progenitors but still present at the floor plate and along some commissural axons, indicating that they probably transported it dorsally (Figure S1H). Next, to study commissural axon pathfinding in *Nes:cre;Ntn1fl/fl* mutants, we performed whole-mount labelling for

Robo3 on E11 embryos followed by 3DISCO clearing and light sheet fluorescent microscopy (LSFM) imaging (Belle et al., 2014). In wild type, a homogenous palisade of thin Robo3+ axonal fascicles extended dorso-ventrally to the floor plate (Figures 1A and 1B; n=6; Movie S1). By contrast, in *Nes:cre;Ntn1^{fl/fl}* E11 embryos (n=6), Robo3+ axons form thick axonal bundles (Figures 1E and 1F and Movie S1). Most Robo3+ axons still reached the floor plate, but unlike in wild type (Figures 1C and 1D), some grew dorsally towards the roof plate, others invaded the VZ and a few left the CNS through the sensory roots (Figures 1G and 1H and Movie S1). Commissural axons were more fasciculated in E11 *Nes:cre;Ntn1^{fl/fl}* embryos (n=8) than in wild type (n=14; Figures 1I-1K and 1M-1O). However, the thickness of the ventral commissure, stained for Robo3, Dcc or Neurofilament was similar to wild type (Figure 1I-K and 1M-O and Figure S3A-C; n=8 embryos). The area of the Robo1+ staining, which is expressed in post-crossing commissural axons, was comparable in wild type and *Nes:cre;Ntn1^{fl/fl}* E11 embryos (Figures 1L and S3G, n=8 and 1P n=7). Interestingly, a small, albeit significant fraction of Robo3+ axons invaded the motor columns (Figures S2A, S2B and S2F, S2G and S3H, n=6). Therefore, a fraction of commissural axons deviate to the motor columns both in *Nes:cre;Ntn1^{fl/fl}* and *Shh:cre;Ntn1^{fl/fl}* but the ventral commissure is only thinner in *Shh:cre;Ntn1^{fl/fl}* embryos, suggesting that in *Shh:cre;Ntn1^{fl/fl}* either axonal growth is slower or that the trajectory followed by commissural axons to the midline is longer than in *Nes:cre;Ntn1^{fl/fl}* embryos. This also shows that at E11, the partial reduction of *Ntn1* expression in the SC VZ, increases commissural axon fasciculation, at least dorsally, but only appears to have a limited effect on their ventral extension.

Many Robo3+ commissural axons cross the midline of *Shh:cre;Ntn1^{fl/fl}* embryos, which lack netrin-1 at the floor plate (Figures S1N-S1P, n=5 for each stage), but their

trajectories have not been examined in detail. LSFM 3D imaging of E11 *Shh:cre;Ntn1^{fl/fl}* spinal cords showed that Robo3+ axons form thin dorso-ventral fascicles as in control embryos (Figure 1Q and Movie S1, n=7) but their organization differs at the midline (Figure 1R, n=7). Unlike in wild type, Robo3+ axons deviated from a straight dorso-ventral path upon reaching the floor plate and gaps devoid of Robo3+ axons were present within the floor plate (Figure 1R and Movie S1). The more vertical trajectory of commissural axons resulted in the overall appearance of the precrossing axons having a U shape (Figures 1U and 1V, n=8) rather than the V shape seen in wild type (Figure 1I-1J). The thickness of the ventral commissure was reduced compared to wild type embryos (Figures 1U-1W and Figure S3A-C). However, the area covered by Robo1+ postcrossing axons was not significantly different from controls and there was no accumulation of Robo1+ axons within the floor plate unlike in other midline mutants (Figure 1X and Figure S3G, n=7)(Long et al., 2004). There was a significant invasion of the motor column by Robo3+ axons (Figure S2K and S2L and Figure S3H). In wild type embryos, double immunostaining for Robo3 and netrin-1 showed that netrin-1 protein was present at the floor plate, in VZ progenitor processes extending to the pial surface and on commissural axons (Figures 1Y and 1Y'). In *Shh:cre;Ntn1^{fl/fl}* embryos netrin-1 was ablated from the floor plate but was still very highly expressed in the adjacent region where Robo3+ axons seemed to accumulate (Figures 1Z and 1Z'). Its distribution at the pial surface and VZ appeared unchanged and it was also present along commissural axons indicating that they might also transport netrin-1 anterogradely (Figure S1Q, n=5). These data show that many commissural axons still reach the ventral midline in absence of floor plate-derived netrin-1 but that their growth in the ventral SC and across the floor plate might be affected.

Next, we studied E13 embryos as new SC commissural neurons are produced until at least until E14 (Comer et al., 2015)(Movie S2). In wild type SC, LSFM imaging showed that Robo3+ axons still formed a well-organized palisade and that Robo3 axon trajectories were straight as they cross the ventral midline (Figures 2A and 2B n=5). The roof plate of the SC did not contain Robo3+ axons (Figures 2C and 2D, n=5). Interestingly, at this stage, Robo3 axons grew ventrally at various depths within the SC and many passed through the motor column (Figures 2E and 2F, n=10), indicating that the avoidance of motor neurons by commissural axons is only a transient feature. In whole-mounts of E13 *Nes:cre;Ntn1^{fl/fl}* SCs, Robo3+ axon trajectories appeared more disorganized, and dorsally, many longitudinal axons were observed together with axons crossing the dorsal midline (Figures 2I-2L, n=6). At this stage, the thickness of the ventral commissure was significantly reduced in *Nes:cre;Ntn1^{fl/fl}* embryos compared to wild type, but only as assessed using Dcc, not Robo3, as a marker (Figures 2E-2H and 2M-2P and Figure S3D-F, n=7). This could either mean that distinct populations of commissural axons are differentially affected by the lack of VZ-derived netrin-1 or could be explained by the distinct expression time-course of Dcc and Robo3, the latter being downregulated just after crossing. As described before in the hindbrain (Moreno-Bravo et al., 2018), a few Robo3+ axons also exited the CNS through the dorsal root ganglia (Movie S2). In *Shh:cre;Ntn1^{fl/fl}* E13 SC, all Robo3 axons extended to the ventral midline as in wild type, but as at E11, their path within the floor plate appeared to be perturbed and distorted (Figures 2Q, 2R and 2T and Movie S2,n=6). The thickness of the ventral commissure was not significantly reduced compared to wild type (Figures 2U-2X and Figure S3D-S3F, n=8). To better visualize commissural axon crossing behavior in *Shh:cre;Ntn1^{fl/fl}* embryos, we injected DiI in the dorsal SC and imaged "open-book" preparations.

Individual axon trajectories (n=443 axons from 4 different wild type embryos and n=497 axons from 4 different *Shh:cre;Ntn1fl/fl* embryos) were reconstructed with ImageJ (see Star methods and Movie S3). In control SCs, commissural axon trajectories and their floor plate entry points were very precisely aligned with only about 1% of axons that deviated more than 30µm from their expected entry point (Figures 3A-3D and 3H). Only 4% of the axons were found to turn on the ipsilateral side (Figure 3D). By contrast, in the SC of *Shh:cre;Ntn1fl/fl* embryos, many axons went astray (Figures 3D-3F). Overall, there was a significant increase of axons that either grew ipsilaterally (4% in wt *vs* 14% in *Shh:cre;Ntn1fl/fl* embryos) or displayed aberrant crossing (3.7% in wt *vs* 22% in *Shh:cre;Ntn1fl/fl* embryos), while the proportion of axons that had not yet crossed the floor plate was comparable (Figure 3D). The position of the floor plate entry point was not aligned with the precrossing trajectory for almost 30% of the traced axons, and for 11.6% the detour exceeded 30µm (Figures 3D and 3G and 3H). For these aberrant axons, the mean turning distance where commissural axons deviated from their expected trajectory, was at 47µm ± 22µm from the floor plate (n=78) (Figures 3G and 3I).

Together, these data show that commissural axons reach the floor plate in *Shh:cre;Ntn1fl/fl* embryos. However, the lack of netrin-1 at the floor plate perturbs their approach and a significant proportion of axons abnormally grow and linger along the floor plate before crossing it. They also show that neither the deletion of netrin-1 from the VZ nor the floor plate is sufficient to recapitulate commissural axon midline crossing defects described in *Ntn1-/-* null mice (Bin et al., 2015; Serafini et al., 1996; Yung et al., 2015). Although this could be explained by the late onset of cre recombinase expression in the VZ of *Nes:cre;Ntn1fl/fl* embryos, it could also suggest that the two netrin-1 sources, the floor plate and VZ, could function redundantly in the

SC. To test this hypothesis, we generated *Nes:cre;Shh:cre;Ntn1$^{fl/fl}$* embryos (n=9 at E11 and n=8 at E13). As expected, *Ntn1* mRNA was reduced but still present in VZ of the double mutant SC at E10 (Figure S1S) but was completely abrogated, as well as netrin-1 protein, in E11 embryos (Figure S1T, U). Strikingly, 3D LSFM imaging of whole-mount SC revealed a severe disorganization of Robo3+ commissural axons in *Nes:cre;Shh:cre;Ntn1$^{fl/fl}$* embryos compare to wild type ones (Figures 4A-4C and Movie S4) including a massive invasion of the motor columns (Figures S2P and S2Q and Figure S3I) and of the dorsal SC (Figures S2C-S2E and S2R-S2T and S2W-S2Y). This dorsal invasion was not observed in *Shh:cre;Ntn1$^{fl/fl}$* embryos (Figure S2M-S2O).The phenotype in *Nes:cre;Shh:cre;Ntn1$^{fl/fl}$* was highly similar to *Ntn1$^{-/-}$* mutants (Figures 4D-4F movie S4, Figure S2U, S2V and Figure S3I, n=5). However, although in both cases a subset of Robo3+ axons exited the CNS, they primarily did it through the dorsal root ganglia in *Ntn1$^{-/-}$* embryos or the motor nerve roots in *Nes:cre;Shh:cre;Ntn1$^{fl/fl}$* embryos (Figure 4A and 4D). The reduction of the ventral commissure and of the Robo1+ post-crossing domain, appeared similar in sections of *Nes:cre;Shh:cre;Ntn1$^{fl/fl}$* and *Ntn1$^{-/-}$* embryos (Figures 4G-4N and Figure S3A-S3C and S3G, n=6 for *Nes:cre;Shh:cre;Ntn1$^{fl/fl}$*, n=7 for *Ntn1$^{-/-}$*). The same observations were made at E13 (Figure 4O-4Z, Figure S3D-S3F). Only a few axon were still able to cross the floor plate in *Nes:cre;Shh:cre;Ntn1$^{fl/fl}$* and *Ntn1$^{-/-}$* embryos and most extended towards the dorsal midline and crossed it, as if the dorsal polarity had been reversed in both mutants (Movie S4).

Discussion

Overlapping and non-redundant function of ventricular zone and floor plate netrin-1

Our results show that netrin-1 from two sources, the floor plate and ventricular zone influence commissural axon guidance in the mouse SC and have overlapping and non-redundant functions. In *Nes:cre;Ntn1fl/fl* mutants, axons are more fasciculated and some also grew dorsally towards the roof plate. In *Shh:cre;Ntn1fl/fl* mutants, which lack netrin-1 at the floor plate, commissural axons still grow ventrally and appear to reach the floor plate, but a significant fraction wander ipsilaterally before reaching the midline and crossing it. In both mutants, the thickness of the ventral commissure is slightly reduced but at different ages. In *Shh:cre;Ntn1fl/fl* embryos, the reduction is significant at E11 but not at E13, and single axon tracing at E13 suggest that this apparent reduction could correspond to a delayed rather than a failure of midline crossing. The rapid drop in netrin-1 level at the floor plate seems to block some commissural axons on the ipsilateral side before their can finally resume crossing. The maintenance, albeit delayed for some axons, of midline crossing, is consistent with earlier findings which showed that floor plate crossing primarily involves repulsive signals such as Slits, and semaphorins, expelling axons from the midline (Chédotal, 2011; Ducuing et al., 2018). By contrast, in *Nes:cre;Ntn1fl/fl* mutants, midline crossing is only reduced at E13, which could be attributed to the late onset of cre activity in this line. Alternatively, the early and late born SC commissural neurons could have distinct requirement for VZ- versus floor plate-netrin-1. Indeed, some late-born commissural neurons located in the dorsal SC, project their axons across the dorsal rather than ventral midline (Comer et al., 2015).

Strikingly, the simultaneous deletion of netrin-1 from VZ and floor plate almost completely abrogate ventral midline crossing, supporting a synergistic contribution of the two sources. The observation that removal of netrin-1 from floor plate

dramatically enhances defects in ventral SC seen after its removal from VZ shows that netrin-1 from floor plate acts within the ventral SC at a distance from the midline. At the same time, these results show that netrin-1 from VZ alone can by itself produce robust guidance since a majority of SC commissural axons cross the floor plate in *Shh:cre;Ntn1^{fl/fl}* embryos. In double mutant embryos, some commissural axons extend dorsally instead of ventrally and cross the dorsal midline, suggesting that dorsal repellents such as BMPs are not sufficient to orient axons ventrally and that netrin-1 might rather prevent commissural axons from wandering dorsally or even potentially being attracted dorsally.

Interestingly, SC commissural axon defects in *Nes:cre;Shh:cre;Ntn1^{fl/fl}* mutants do not fully phenocopy netrin-1 null mice. Midline crossing is equally reduced, but whereas a subset of commissural axons leaves the CNS through DRGs in *Ntn1^{-/-}* embryos, they primarily escape through motor nerve roots in *Nes:cre;Shh:cre;Ntn1^{fl/fl}* embryos. This suggests that some netrin-1, from a third source, might still be detected by commissural axons in these mutants. This third source of netrin-1 could be motor neurons, which express Dcc and whose axons are guided by netrin-1 in the periphery. Netrin-1 could be transported retrogradelly along motor axons that could then provide an alternative netrin-1 substrate for misguided commissural axons. Accordingly, we could detect netrin-1 immunoreactivity on motor nerves in *Nes:cre;Shh:cre;Ntn1^{fl/fl}* embryos (data not shown).

Does netrin-1 influence commissural axon fasciculation?

Our 3D analysis of guidance defects in *netrin-1* conditional mutants, suggests that netrin-1 levels might influence commissural axon fasciculation. SC commissural axons normally grow straight and perpendicular to the floor plate but the occurrence

of contacts and avoidance between precrossing commissural axons has been previously described in zebrafish (Moon and Gomez, 2005). First, we found that commissural axons form compact dorso-ventral fascicles in *Nes:cre;Ntn1^{fl/fl}* embryos, not seen in wild type. In addition, commissural axons in *Shh:cre;Ntn1^{fl/fl}* embryos, deviate from their expected trajectory in the floor plate vicinity suggesting that they are less attracted by floor plate or that they might prematurely defasciculate.

Second, in *Nes:cre;Ntn1^{fl/fl}* and *Shh:cre;Ntn1^{fl/fl}* E11 embryos, a small fraction of commissural axons deviate from their normal trajectory to grow across the motor columns, a phenotype much more pronounced in double conditional mutants and *netrin-1* null embryos. This could support the existence of a chemoattractive gradient of netrin-1 diffusing from floor plate but could also be explained by a defasciculation of commissural axons upon entering the ventral SC. Previous in vitro studies support short-range/haptotatic growth promoting function of substrate-bound netrin-1 (Moore et al., 2009). Interestingly, the recent structural analysis of the draxin/netrin/Dcc tripartite molecular complex, also suggests that draxin (dorsal repulsive axon guidance protein) (Islam et al., 2009) and netrin, which bind each other (Gao et al., 2015), might influence the fasciculation of Dcc-expressing axons (Liu et al., 2018).

Floor plate has distinct axon guidance function in hindbrain and SC

In the mouse hindbrain, the absence of netrin-1 from the VZ but not the floor plate severely alters midline crossing (Dominici et al., 2017; Yamauchi et al., 2017). Here, we show that this is not the case in the SC. Although the incomplete inactivation of VZ-netrin-1 could have explained the moderate commissural axon defects in the SC of *Nes:cre;Ntn1^{fl/fl}* embryos, the major reduction of midline crossing in *Nes:cre;Shh:cre;Ntn1^{fl/fl}* double mutants rather supports a compensatory/redundant

role of floor plate-netrin-1. This suggests that the floor plate has distinct influences on commissural axons in the hindbrain and the SC. This hypothesis is supported by the recent analysis of commissural neuron development in conditional knockout mice lacking all Slits at the floor plate (Dominici et al., 2018). In these mutants, only SC commissural axons exhibit midline crossing defects compatible with a Slit-dependent repulsive activity of floor plate whereas they develop normally in the hindbrain. What could explain this difference? The size and volume of the hindbrain at the time commissural axons develop, is much larger than the SC, and nascent growth cones would be located too far from the floor plate to be influenced by it. Finding the ventral midline only through a netrin-1 gradient would be particularly challenging in larger vertebrate species, such as primates and therefore, an alternative and more dorsal netrin-1 source, the ventricular zone, might have become preponderant in the mammalian hindbrain. Although, existing data do not allow to date phylogenetically the appearance of VZ-netrin-1, in the Amphioxus CNS, netrin-1 seems to be restricted to the floor plate in the SC but extends more dorsally at more rostral levels (Shimeld, 2000). Together these data suggest that commissural axon guidance mechanisms differ between the hindbrain and SC.

Acknowledgments

Author contributions

Conceptualization, A.C.; Methodology, A.C. and P.M.; Investigation, J.A.M.B. and S.R.P; Writing – Original draft, A.C.; Writing – Reviews & Editing, PM, J.A.M.B. and S.R.P.; Visualization, A.C., J.A.M.B. and S.R.P.; Supervision, A.C.; Resources, P.M.; Funding acquisition, A.C.; Project administration, A.C..

Declaration of Interest

The authors declare no competing of interest.

References

Belle, M., Godefroy, D., Dominici, C., Heitz-Marchaland, C., Zelina, P., Hellal, F., Bradke, F., and Chédotal, A. (2014). A Simple Method for 3D Analysis of Immunolabeled Axonal Tracts in a Transparent Nervous System. Cell Rep. *9*, 1191–1201.

Belle, M., Godefroy, D., Couly, G., Malone, S.A., Collier, F., Giacobini, P., and Chédotal, A. (2017). Tridimensional Visualization and Analysis of Early Human Development. Cell *169*, 161–173.e12.

Bin, J.M., Han, D., Lai Wing Sun, K., Croteau, L.-P., Dumontier, E., Cloutier, J.-F., Kania, A., and Kennedy, T.E. (2015). Complete Loss of Netrin-1 Results in Embryonic Lethality and Severe Axon Guidance Defects without Increased Neural Cell Death. Cell Rep. *12*, 1099–1106.

Charron, F., Stein, E., Jeong, J., McMahon, A.P., and Tessier-Lavigne, M. (2003). The morphogen sonic hedgehog is an axonal chemoattractant that collaborates with netrin-1 in midline axon guidance. Cell *113*, 11–23.

Chédotal, A. (2011). Further tales of the midline. Curr. Opin. Neurobiol. *21*, 68–75.

Chédotal, A. (2014). Development and plasticity of commissural circuits: from locomotion to brain repair. Trends Neurosci. *37*, 551–562.

Comer, J.D., Pan, F.C., Willet, S.G., Haldipur, P., Millen, K.J., Wright, C.V.E., and Kaltschmidt, J. a. (2015). Sensory and spinal inhibitory dorsal midline crossing is independent of Robo3. Front. Neural Circuits *9*, 1–14.

Dominici, C., Moreno-Bravo, J.A., Puiggros, S.R., Rappeneau, Q., Rama, N., Vieugue, P., Bernet, A., Mehlen, P., and Chédotal, A. (2017). Floor-plate-derived netrin-1 is dispensable for commissural axon guidance. Nature *545*, 350–354.

Dominici, C., Rappeneau, Q., Zelina, P., Fouquet, S., and Chédotal, A. (2018). Non-cell autonomous control of precerebellar neuron migration by Slit and Robo proteins. Development *145*, dev.150375.

Ducuing, H., Gardette, T., Pignata, A., Tauszig-Delamasure, S., and Castellani, V. (2018). Commissural axon navigation in the spinal cord: A repertoire of repulsive forces is in command. Semin. Cell Dev. Biol. 1–10.

Fazeli, A., Dickinson, S.L., Hermiston, M.L., Tighe, R. V, Steen, R.G., Small, C.G., Stoeckli, E.T., Keino-Masu, K., Masu, M., Rayburn, H., et al. (1997). Phenotype of mice lacking functional Deleted in colorectal cancer (Dcc) gene. Nature *386*, 796–804.

Gao, X., Metzger, U., Panza, P., Mahalwar, P., Alsheimer, S., Geiger, H., Maischein, H.-M., Levesque, M.P., Templin, M., and Söllner, C. (2015). A Floor-Plate Extracellular Protein-Protein Interaction Screen Identifies Draxin as a Secreted Netrin-1 Antagonist. Cell Rep. *12*, 694–708.

Goodman, C.S. (1996). Mechanisms and Molecules that Control Growth Cone Guidance. Annu. Rev. Neurosci. *19*, 341–377.

Harfe, B.D., Scherz, P.J., Nissim, S., Tian, H., McMahon, A.P., and Tabin, C.J. (2004). Evidence for an Expansion-Based Temporal Shh Gradient in Specifying Vertebrate Digit Identities. Cell *118*, 517–528.

Islam, S.M., Shinmyo, Y., Okafuji, T., Su, Y., Naser, I. Bin, Ahmed, G., Zhang, S., Chen, S., Ohta, K., Kiyonari, H., et al. (2009). Draxin, a repulsive guidance protein for spinal cord and forebrain commissures. Science *323*, 388–393.

Kennedy, T.E., Serafini, T., de la Torre, J., and Tessier-Lavigne, M. (1994). Netrins are diffusible chemotropic factors for commissural axons in the embryonic spinal cord. Cell *78*, 425–435.

Kennedy, T.E., Wang, H., Marshall, W., and Tessier-Lavigne, M. (2006). Axon guidance by diffusible chemoattractants: a gradient of netrin protein in the developing spinal cord. J. Neurosci. *26*, 8866–8874.

Liu, Y., Bhowmick, T., Liu, Y., Gao, X., Mertens, H.D.T., Svergun, D.I., Xiao, J., Zhang, Y., Wang, J., and Meijers, R. (2018). Structural Basis for Draxin-Modulated Axon Guidance and Fasciculation by Netrin-1 through DCC. Neuron *97*, 1261–1267.e4.

Long, H., Sabatier, C., Ma, L., Plump, A.S., Yuan, W., Ornitz, D.M., Tamada, A., Murakami, F., Goodman, C.S., and Tessier-Lavigne, M. (2004). Conserved roles for Slit and Robo proteins in midline commissural axon guidance. Neuron *42*, 213–223.

Marillat, V., Cases, O., Nguyenf-Ba-Charvet, K.T., Tessier-Lavigne, M., Sotelo, C., and Chédotal, A. (2002). Spatiotemporal expression patterns of slit and robo genes in the rat brain. J. Comp. Neurol. *442*, 130–155.

Moon, M.-S., and Gomez, T.M. (2005). Adjacent pioneer commissural interneuron growth cones switch from contact avoidance to axon fasciculation after midline crossing. Dev. Biol. *288*, 474–486.

Moore, S.W., Biais, N., and Sheetz, M.P. (2009). Traction on Immobilized Netrin-1 Is Sufficient to Reorient Axons. Science *325*, 166–166.

Moreno-Bravo, J.A., Puiggros, S.R., Blockus, H., Dominici, C., Zelina, P., Mehlen, P., and Chédotal, A. (2018). Commissural neurons transgress the CNS/PNS boundary in absence of ventricular zone-derived netrin-1. Development *145*, dev.159400.

Okada, A., Charron, F., Morin, S., Shin, D.S., Wong, K., Fabre, P.J., Tessier-Lavigne, M., and Mcconnell, S.K. (2006). Boc is a receptor for sonic hedgehog in the guidance of commissural axons. Nature *444*, 369–373.

Ramón y Cajal, S. (1892). La rétine des vertébrés. Cellule *1*, 119–257.

Ruiz de Almodovar, C., Fabre, P.J., Knevels, E., Coulon, C., Segura, I., Haddick, P.C.G., Aerts, L., Delattin, N., Strasser, G., Oh, W.-J., et al. (2011). VEGF Mediates Commissural Axon Chemoattraction through Its Receptor Flk1. Neuron *70*, 966–978.

Serafini, T., Kennedy, T.E., Gaiko, M.J., Mirzayan, C., Jessell, T.M., and Tessier-Lavigne, M. (1994). The netrins define a family of axon outgrowth-promoting proteins homologous to C. elegans UNC-6. Cell *78*, 409–424.

Serafini, T., Colamarino, S.A., Leonardo, E.D., Wang, H., Beddington, R., Skarnes, W.C., and Tessier-Lavigne, M. (1996). Netrin-1 is required for commissural axon guidance in the developing vertebrate nervous system. Cell *87*, 1001–1014.

Shimeld, S. (2000). An amphioxus netrin gene is expressed in midline structures during embryonic and larval development. Dev. Genes Evol. *210*, 337–344.

Tessier-Lavigne, M., Placzek, M., Lumsden, A.G., Dodd, J., and Jessell, T.M. (1988). Chemotropic guidance of developing axons in the mammalian central nervous system. Nature *336*, 775–778.

Tronche, F., Kellendonk, C., Kretz, O., Gass, P., Anlag, K., Orban, P.C., Bock, R., Klein, R., and Schütz, G. (1999). Disruption of the glucocorticoid receptor gene in the

nervous system results in reduced anxiety. Nat. Genet. *23*, 99–103.

Varadarajan, S.G., Kong, J.H., Phan, K.D., Kao, T.-J., Panaitof, S.C., Cardin, J., Eltzschig, H., Kania, A., Novitch, B.G., and Butler, S.J. (2017). Netrin1 Produced by Neural Progenitors, Not Floor Plate Cells, Is Required for Axon Guidance in the Spinal Cord. Neuron *94*, 790–799.e3.

Voiculescu, O., Charnay, P., and Schneider-Maunoury, S. (2000). Expression pattern of aKrox-20/Cre knock-in allele in the developing hindbrain, bones, and peripheral nervous system. Genesis *26*, 123–126.

Xu, K., Wu, Z., Renier, N., and Antipenko, A. (2014). Structures of netrin-1 bound to two receptors provide insight into its axon guidance mechanism. Science *344*, 1275–1279.

Yamauchi, K., Yamazaki, M., Abe, M., Sakimura, K., Lickert, H., Kawasaki, T., Murakami, F., and Hirata, T. (2017). Netrin-1 Derived from the Ventricular Zone, but not the Floor Plate, Directs Hindbrain Commissural Axons to the Ventral Midline. Sci. Rep. *7*, 11992.

Yung, A.R., Nishitani, A.M., and Goodrich, L. V. (2015). Phenotypic analysis of mice completely lacking netrin 1. Development *142*, 3686–3691.

Yung, A.R., Druckenbrod, N.R., Cloutier, J.-F., Wu, Z., Tessier-Lavigne, M., and Goodrich, L. V. (2018). Netrin-1 Confines Rhombic Lip-Derived Neurons to the CNS. Cell Rep. *22*, 1666–1680.

Figure legends

Figure 1

Distinct commissural axon guidance defects following netrin-1 depletion from ventricular zone or floor plate.

All images are from E11 embryos and dotted lines indicate the midline. (A-H) LSFM images of the SC of wild type (A-D) and *Nes:cre;Ntn1^{fl/fl}* embryos (E-H) immunolabelled for Robo3. Robo3+ commissural axons are more fasciculated in *Nes:cre;Ntn1^{fl/fl}* (arrows in E, F) mutant than in wild type (A, B) and some invade the dorsal SC (arrowheads in G, H) and motor columns (asterisks in D, H). (I-P) Confocal images of coronal SC sections at the brachial level. The ventral commissure (arrow) labelled for Robo3 (I, M), Dcc (J, N) or Neurofilament (K, O) is not reduced in *Nes:cre;Ntn1^{fl/fl}* (M-O) compared to wild type (I-K), but pre-crossing axons are more fasciculated (arrowheads in M and N). Robo1 labels post-crossing axons (arrows in L, P) and a subset of pre-crossing commissural axons (arrowheads in L, P). The floor plate is labelled with Alcam (K, O). (Q-T) LSFM images of *Shh:cre;Ntn1^{fl/fl}* embryos immunolabelled for Robo3. Robo3+ axons reach the floor plate but some follow it and go astray during crossing (arrowheads in Q and R). They do not grow toward the dorsal midline (S). (U-Z') Confocal images of coronal SC sections at the brachial level. The ventral commissure labelled with Robo3 (U, Z) or Dcc (V) has an abnormal "U" shape in *Shh:cre;Ntn1^{fl/fl}* embryos. Neurofilament (W) and Robo1 (X) staining are similar to wild type. In wild type (Y, Y') netrin-1 protein is found at the floor plate, on VZ precursors (arrowheads) and commissural axons (arrow). *Shh:cre;Ntn1^{fl/fl}* embryos (Z, Z') lack floor plate-netrin-1 and Robo3 axons extend more laterally, closer to the pial surface where netrin-1 is still present (arrows in Z, Z').

Scale bars: 100 μm (A, C, D, E, F, G, H, Q, S and T) and 50μm (all other panels).

See also Figure S3 for quantification and Movie S1

Figure 2

Commissural axons invade the dorsal spinal cord in absence of ventricular-zone-derived netrin-1

All images are from E13 embryos and dotted lines indicate the midline. (A-D, I-L and Q-T) LSFM images of SCs labelled for Robo3. (E-H, M-P and U-X) Coronal sections at the brachial level labelled for Islet1 and Robo3 (E, M, U), Robo3 (F, N, V), Dcc (G, O, W) or Neurofilament (H, P, X). In wild type (A-H), all Robo3+ axons extend ventrally (A-F) and some cross the Islet1+ motor columns (arrowheads in E, F). In *Nes:cre;Ntn1fl/fl* embryos (I-P) the ventral trajectory of Robo3+ axons is irregular (arrowheads in I) and they are misguided in the dorsal SC (K). The ventral commissure (arrow N-P) is slightly reduced compared with wild type (arrow in F-H). In *Shh:cre;Ntn1fl/fl* embryos (Q-X) Robo3 axons reach the floor plate but adopt a distorted path during crossing (arrowheads in Q). The thickness of the ventral commissure (arrows in V-X) is comparable to wild type. See also Figure S3 for quantification and Movie S2.

Scale bars: 100 µm (A, C, D, I, K, L, Q, S and T) and 50µm (all other panels).

Figure 3

Abnormal midline crossing in absence of netrin-1 at the floor-plate

(A, B, E, F) Confocal images of E13 SC "open book" preparations of wild type (A, B) and *Shh:cre;Ntn1fl/fl* (E, F) embryos injected dorsally with DiI. The lines delineate the floor plate. Only a few axons illustrating the diverse crossing behaviors are colorized (see methods). (C) Schematic representation of the various types of commissural axon behaviors at the midline. (D) Quantification of midline crossing behaviors. The graphs represent the frequency of axon crossing behaviors as a percentage. Results are significant (*) for p-value < 0.05. (G) Diagram illustrating the quantification procedure of the aberrant turning point and midline entry point. (H) Distances (µm) separating the floor plate expected entry point and the observed entry point for

individual axons. In *Shh:cre;Ntn1^{fl/fl}* (blue) a significant portion of precrossing axons grow ipsilaterally along the floor plate before crossing it. (I) Quantification of the commissural axon turning point distance in *Shh:cre;Ntn1^{fl/fl}* embryos. See also movie S3.

Scale bars: 30µm in (A, B, E and F)

Figure 4

The simultaneous deletion of netrin-1 from the floor plate and VZ leads to severe midline crossing defects.

(A-F and O-T) LSFM images of E11 (A-F) and E13 (O-T) SCs labelled for Robo3 where the dotted lines indicate the midline. (G-N and U-Z) Coronal sections at the brachial level labelled for Robo3 (G, K, U', X'), Robo3 and Islet1 (U, X), Dcc (H, L, V, Y), Robo1 (J, N) or Neurofilament (I, M, W, Z). In E11 *Nes:cre;Shh:cre;Ntn1^{fl/fl}* (A-C, G-J) and *Ntn1^{-/-}* (D-F, K-N) embryos, SC commissural axons are severely misguided to the ventral midline (A, D) and extensively spread over the dorsal SC (arrowheads in B, C, E, F). Arrows in (C) and (F) indicate Robo3 axons leaving the CNS via motor nerve roots (C) or dorsal root ganglia (F). (G-N) in both mutants, the ventral commissure is almost absent and commissural axons invade the motor column (asterisk in C, F, G, K). (O-Z) At E13, only a few commissural axons are able to cross the floor plate (arrowheads in O, R, U-W and X-Z). Dorsally, Robo3+ axons massively cross the midline in *Nes:cre;Shh:cre;Ntn1^{fl/fl}* mutants (arrowheads in P and Q). In *Ntn1^{-/-}*, dorsal crossing is more limited (arrowheads in S) but axons appear to extend longitudinally (arrows in S). At this stage, only a few axons cross the ventral commissure in mutant embryos (arrowheads in U-Z).

See also Figure S3 for quantification and Movie S4.

Scale bars: 100 µm (A, B, C, D, E, F, O, P, R, S and T) and 50µm (all other panels).

STAR Methods

Contact for Reagent and Resource Sharing

Further information and requests for resources and reagents should be directed to and will be fulfilled by the Lead Contact, Alain Chédotal (alain.chedotal@inserm.fr).

Experimental Model and Subject Details

Generation and analysis of mutant embryos

The following mouse strains were used: *Netrin1* conditional knockout (*Ntn1^fl*)(Dominici et al., 2017), *Shh:cre* (Harfe et al., 2004), *Nestin:cre (Nes:cre)* (Tronche et al., 1999) and *Ai9 RosatdTomato (Rosa^Tom*; Jackson lab*). Ntn1^-/-* mice we obtained by crossing *Netrin-1^fl/fl* and *Krox20:cre* mice which express Cre recombinase in the male and female germline after sexual maturity (Voiculescu et al., 2000). Genotypes were determined by PCR using tail genomic DNA. The day of vaginal plug was counted as embryonic day 0.5 (E0.5). Embryos of either sex were used and size. Mice were handled and housed in accordance to institutional guidelines and approved by the Charles Darwin Ethics Committee of Sorbonne Université.

Method Details

Immunohistochemistry

Embryos were fixed in 4% paraformaldehyde (PFA) in 0.12 M phosphate buffer, pH 7.4 at 4°C overnight (O/N), cryoprotected in sucrose 10%, frozen in isopentane and sectioned at 20 µm. Sections were blocked in PBS-gelatin (0,2%, PBS-GT) containing 0,25% Triton-X 100 (Sigma-Aldrich) and incubated in the following primary

antibodies at room temperature (RT) overnight: goat anti-human Robo3 (1:500, R&D Systems AF3076), goat anti-Robo1 (1:200, R&D Systems AF1749), goat anti-Dcc (1:500, Santa Cruz sc-6535), rabbit anti-Islet1 (1:1000, Abcam AB20670) rat anti-mouse netrin-1 (1:1000, R&D Systems MAB1109), rabbit anti-DsRed (1:1000, Clontech 632496), mouse anti-neurofilament (1:500, DSHB 2H3), goat anti-human ALCAM (1:500, R&D Systems AF656), rabbit anti-DsRed (1:500, Clontech 632496). The netrin1 antibody signal was increased by using an antigen retrieval method. The sections were boiled in citrate buffer (pH6) during 5 minutes before the blocking step. Species-specific secondary antibodies conjugated to Alexa-Fluor fluorophores from Jackson ImmunoResearch or Invitrogen were used after the primary antibodies incubation. The sections were counterstained with DAPI (1:1,000, Sigma-Aldrich). The slides were scanned with a Nanozoomer (Hamamatsu) and confocal microscope (FV1000, Olympus) and processed using ImageJ (NIH) and Adobe Photoshop CS6.

Whole-mount immunostaining and clearing procedure

Whole E11 and E13 SCs were immunostained and cleared as described (Belle et al., 2014, 2017). Briefly, after dehydration in methanol, the SCs were bleached using 6% hydrogen peroxide solution in 100% methanol O/N at 4°C. Samples were blocked using PBS-GT containing 0.5% Triton X-100 (Sigma-Aldrich) O/N at RT and then incubated for 5 days at 37ºC with Robo3 antibody (1:300, R&D Systems AF3076). This was followed by six washes of 30 min in PBSGT 0.5% at RT and incubated with the secondary antibody O/N at 37ºC.

Image Processing

3D imaging was performed with a light-sheet fluorescence microscope (Ultramicroscope I, LaVision BioTec) using Inspector Pro software (LaVision BioTec). Images and 3D volume were generated using Imaris ×64 software (Bitplane).

DiI tracing

E13 spinal cords were fixed in 4% PFA in an open book configuration. 1,1'-dioctadecyl-3,3,3',3'-tetramethylindo-carbocyanine perchlorate (DiI, Invitrogen) diluted in dimethyl sulfoxide (DMSO, Sigma-Aldrich) was injected into the dorsal spinal cord using a glass micropipette. Flat-mounts were kept for 72 h at RT in 4% PFA. The images were acquired with a confocal microscope (FV1000, Olympus)

In each confocal stack images, as many individual axons as possible were traced using the "Simple Neurite tracer" plugin of NIH ImageJ from confocal microscope images. Moreover, using the Imaris (Bitplane) surface tool, single axons were also manually selected and pseudo-colored (Figures 3B and 3F).

In situ hybridization

The Ntn1 exon3 specific antisense RNA probe was labelled with digoxigen-11-d-UTP (Roche diagnostics) as described elsewhere (Marillat et al., 2002) by *in vitro* transcription of cDNA encoding for the exon of interest (Dominici et al., 2017).

Quantification and Statistical analysis

Any statistical method was used to predetermine sample sizes and we did not perform randomization into groups. An observer blinded to the experimental conditions realized all the quantifications. All the data are represented as mean values ± SD. Statistical significance was estimated using one-sided unpaired tests for

non-parametric tendencies (Kruskall-Wallis or Mann-Whitney) and differences were considered significant for p-value < 0.05.

The thickness of the ventral commissure was quantified using at least 5 sections of brachial spinal cord per embryo. To minimize the developmental variations, every section value was normalized towards the height of the spinal cord (Figure S3A-S3F)(Xu et al., 2014).

The area occupied by the Robo1 post-commissural bundle was quantified like the ventral commissure. In this case, to minimize the developmental variations between embryos, every section value was normalized to the total surface of the spinal cord (Figure S3G).

Finally, the invasion of the motor column by Robo3+ axons was also quantified using 5 sections per embryo at the brachial level. In this case, the developmental variability was reduced normalizing the values to the selected spinal cord motor surface (Figure S3H)(Charron et al., 2003; Ruiz de Almodovar et al., 2011).

In all graphical representations, each point represents one of the 5 sections of an embryo. To compare with control cases, the ratios of the different quantifications were normalized to the mean of the controls. At least 5 embryos of each genotype and from 3 different litters were quantified.

The axonal trajectories in wild type and *Shh:cre;Ntn1^{fl/fl}* were quantified by tracing axons of two independent DiI injections from 4 different cases. To determine the proportion of the different axonal behaviors (inside, crossing, ipsilateral and aberrant crossing) a total of 443 and 497 axons were analyzed in the two respective genotypes (Figure 3D). To determine the distance from the expected entry point respect to the real entry point in the floor plate we studied dorso-ventral trajectories of 411 axon in the wild type and 447 axons in the *Shh:cre;Ntn1^{fl/fl}* (Figure 3H and 3I).

Last, for the 78 aberrant crossing axons in the *Shh:cre;Ntn1fl/fl* we determined the turning point distance from the floor plate (Figure 3I)

Data and software availability

The data that supports the findings of this study are available from the lead author upon reasonable request.

All statistical analyses, means and variance calculations were performed using Microsoft Excel and Graphpad Prism7 software. See Key Resources Table for information regarding other softwares used.

Supplemental videos

Movie S1. Related to Figure 1. 3D movie of cleared spinal cords from E11 wild type, *Nes:cre;Ntn1fl/fl* and *Shh:cre;Ntn1fl/fl* embryos illustrating the different commissural axons defects (Robo3 immunostaining).

Movie S2. Related to Figure 2. 3D movie of cleared spinal cords from E13 wild type, *Nes:cre;Ntn1fl/fl* and *Shh:cre;Ntn1fl/fl* embryos illustrating the different commissural axons defects (Robo3 immunostaining).

Movie S3 Related to Figure 3. DiI injections in open book" preparations of E13 wild type and *Shh:cre;Ntn1fl/fl* embryos illustrating the abnormal midline crossing in absence of floor plate netrin-1.

Movie S4. Related to Figure 4. 3D movie of cleared spinal cords from E11 and E13 *Nes:cre;Shh:cre;Ntn1fl/fl* and *Ntn1-/-* embryos illustrating the severe reduction of midline crossing and invasion of the dorsal spinal cord by Robo3+ axons.

Floor plate view — *Roof plate view* — *Oblique (3D)*

Wild type (A–D): Robo3

Nes:cre;Ntn1^{fl/fl} (E–H)

Wild type (I–L): Robo3, Dcc, NF Alcam, Robo1

Nes:cre;Ntn1^{fl/fl} (M–P)

Shh:cre;Ntn1^{fl/fl} (Q–T): Robo3

Shh:cre;Ntn1^{fl/fl} (U–X): Robo3, Dcc, NF Alcam, Robo1

Wild type (Y, Y') — **Shh:cre;Ntn1^{fl/fl}** (Z, Z'): Robo3 Netrin-1

Floor plate view | | *Roof plate view* | *Oblique (3D)*

Wild type — Robo3 (A, B, C, D); Robo3/Islet1, Robo3, Dcc, NF (E, F, G, H)

Nes:cre;Ntn1^{fl/fl} (I, J, K, L, M, N, O, P)

Shh:cre;Ntn1^{fl/fl} (Q, R, S, T, U, V, W, X)

Labels: Robo3 (red) / Islet1 (green); Robo3; Dcc; NF; E13

Wild type

A E13 DiI

B E13 DiI
FP

C
FP
dSC
Inside Crossing Ipsilateral Aberrant Crossing
P ———————————————————————→ A

D
% of total n° of axons

□ *Ntn1*^(fl/fl)
▨ *Shh:cre; Ntn1*^(fl/fl)

ns   *   *   *

Shh:cre; Ntn1^(fl/fl)

E E13 DiI
FR

F E13 DiI
FR

G
FP
expected entry-point   Represented distance   aberrant entry-point
Turning point
dSC

H
% of total number of axons
99.02% 88.36%

■ *Ntn1*^(fl/fl)
■ *Shh:cre; Ntn1*^(fl/fl)

Distance from the expected entry point (µm)

I *Shh:cre; Ntn1*^(fl/fl)
Turning point distance from the floor plate (µm)
FP
dSC

Floor plate view   *Roof plate view*   *Oblique (3D)*

KEY RESOURCES TABLE

REAGENT or RESOURCE	SOURCE	IDENTIFIER
Antibodies		
Goat polyclonal anti-Human ROBO3	R and D Systems	Cat# AF3076; RRID:AB_2181865
Goat anti-Rat ROBO1	R and D Systems	Cat# AF1749, RRID:AB_354969
Goat anti-Human DCC (A-20)	Santa Cruz Biotechnology	Cat# sc-6535, RRID:AB_2245770
Goat anti-Human Alcam	R and D Systems	Cat# AF656, RRID:AB_355509
Rabbit polyclonal anti-Human Islet1	Abcam	Cat# ab20670; RRID:AB_881306
Rabbit anti-DsRed	Clontech Laboratories, Inc.	Cat# 632496, RRID:AB_10013483
Mouse anti-Mouse Neurofilament	DSHB	Cat# 2H3, RRID:AB_531793
Rat anti-Mouse Netrin1	R and D Systems	Cat# MAB1109, RRID:AB_2154710)
Bacterial and Virus Strains		
Biological Samples		
Chemicals, Peptides, and Recombinant Proteins		
Critical Commercial Assays		
Deposited Data		
Experimental Models: Cell Lines		
Experimental Models: Organisms/Strains		
Mouse: Ntn1 flox (conditional knockout)	Dominici et al., 2017	N/A
Mouse: Krox20:cre	Voiculescu O. et al 2000	N/A
Mouse: B6.Cg-Tg(Nes-cre)1Kln/J	Jackson Laboratories	Cat# JAX:003771, RRID:IMSR_JAX:003771
Mouse: B6.Cg-Shhtm1(EGFP/cre)Cjt/J	Jackson Laboratories	Cat# JAX:005622, RRID:IMSR_JAX:005622)
Mouse: B6.Cg-Gt(ROSA)26Sortm9(CAG-tdTomato)Hze/J	Jackson Laboratories	Cat# JAX:007909, RRID:IMSR_JAX:007909)

Oligonucleotides		
In situ probe for Ntn1 exon3: forward 5'-ATGATGCGCGCTGTGTGG-3', reverse 5'-AGCTCCGAGTCGTCTTCG-3', SP6 site	Dominici et al., 2017	NA
Recombinant DNA		
Software and Algorithms		
Adobe Photoshop CS6/CC	Adobe	RRID:SCR_014199)
Adobe Illustrator CS5/CC	Adobe	RRID:SCR_010279
Graphpad Prism7	Graphpad	RRID:SCR_002798 https://www.graphpad.com/
Inspector Pro	LaVision BioTec	N/A
Imaris x64 v8	Bitplane	RRID:SCR_007370) http://www.bitplane.com/download#imaris
NDP.view2	Hamamatsu	N/A https://www.hamamatsu.com/eu/en/product/type/U12388-01/index.html
Fluoview FV10-ASW	Olympus	RRID:SCR_014215 https://www.olympus-lifescience.com/en/support/downloads/#!dlOpen=%23detail847249651
ImageJ	NIH	RRID:SCR_003070 https://imagej.nih.gov/ij/download.html
IMovie	Apple	https://support.apple.com/downloads/imovie
Other		

Supplemental Information

Synergistic activity of floor plate and ventricular zone-derived netrin-1 in spinal cord commissural axon guidance

Juan Antonio Moreno-Bravo, Sergi Roig Puiggros, Patrick Mehlen and Alain Chédotal

Wild type

A E9 — Ntn1ex3 *
B E10 — Ntn1ex3 *
C E11 — Ntn1ex3 *
D E11 — Ntn1

Nes:cre;Ntn1fl/fl

E E9 — Ntn1ex3 *
F E10 — Ntn1ex3 *
G E11 — Ntn1ex3 *
H E11 — Ntn1

Nes:cre;RosaTom

I E9 — Dsred
J E10 — Dsred
K E11 — Alcam Dsred
L Dsred Alcam *
M Dsred

Shh:cre; Ntn1fl/fl

N E9 — Ntn1ex3 *
O E10 — Ntn1ex3 *
P E11 — Ntn1ex3 *
Q E11 — Ntn1

Ntn1-/-

R E11 — Ntn1ex3

Nes:cre;Shh:cre;Ntn1fl/fl

S E10 — Ntn1ex3
T E11 — Ntn1ex3
U E11 — Ntn1
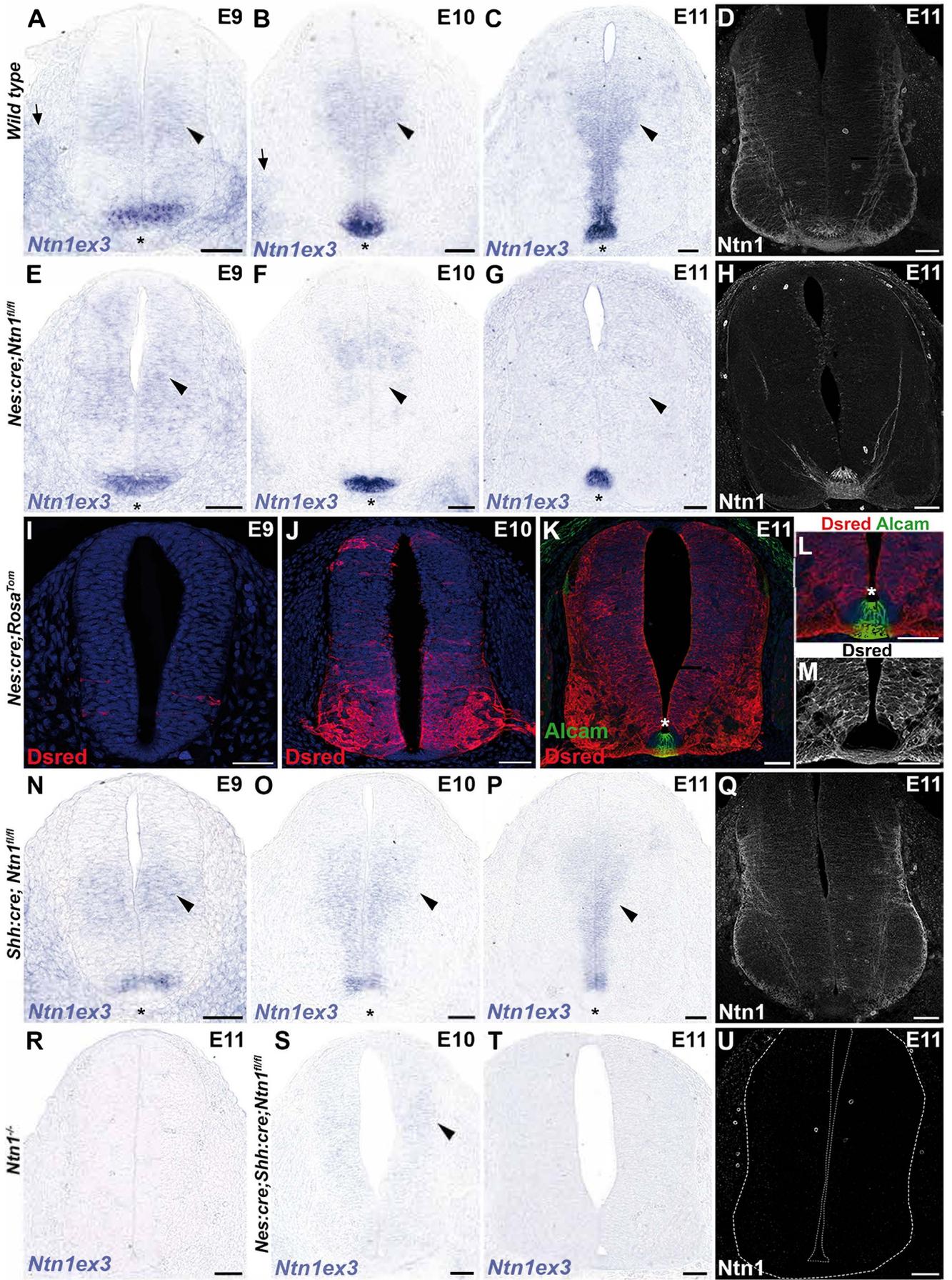
Figure S1 (Related to **Figure 1** and **Figure 4)**

Netrin-1 expression in VZ-specific, floor plate-specific and compound *netrin-1* mutants.

(A-U) Coronal cryostat sections of the brachial spinal cord of E9, E10 and E11 embryos. (A-C, E-G, N-P and R-T) In situ hybridization for *netrin-1 exon 3*. (D,H,Q,U) netrin-1 immunostaining. (A-C) In wild type, netrin-1 mRNA is found in the floor plate (asterisk) and VZ (arrowheads) and also, at E9 and E10, in surrounding mesenchyme (arrow in A and B). In wild type, netrin-1 is present at the pial surface and on commissural axons (D). (E-G) In *Nes:cre;Ntn1$^{fl/fl}$* embryos, *netrin-1* is maintained at the floor plate (asterisk) but progressively deleted from the VZ from E10 (arrowheads). At E11, netrin-1 is only detected on commissural axons and floor plate (H). (I-M) are sections from *Nes:cre;Rosa^{Tom}* embryos illustrating the progressive cre activation in the spinal cord VZ. Note the absence of Tomato expression at the floor plate (asterisk) labelled with Alcam in K and L. (N-P) In *Shh:cre;Ntn1$^{fl/fl}$* embryos, netrin-1 mRNA is deleted from the floor plate (asterisk) but unchanged in the VZ (arrowheads). At E11, netrin-1 protein is still detectable at the pial surface and on commissural axons (Q). (R-T) Netrin-1 is absent in *Ntn1$^{-/-}$* null embryos (R) and in *Nes:cre;Shh:cre;Ntn1$^{fl/fl}$* netrin-1 expression is almost abrogated at E10 (arrowhead in S) and undetectable at E11 (T). Netrin-1 is absent in the spinal cord of the compound mutant (U). The dotted line delineates the spinal cord.

Scale bars: 50 µm in all panels.

Robo3 Islet1 | Robo3 | Dcc | Robo3

Wild type

A E11 B C D E E13

Nes:cre;Ntn1^{fl/fl}

F G H I J

Shh:cre;Ntn1^{fl/fl}

K L M N O

Nes:cre;Shh:cre;Ntn1^{fl/fl}

P Q R S T

Ntn1-/-

U V W X Y
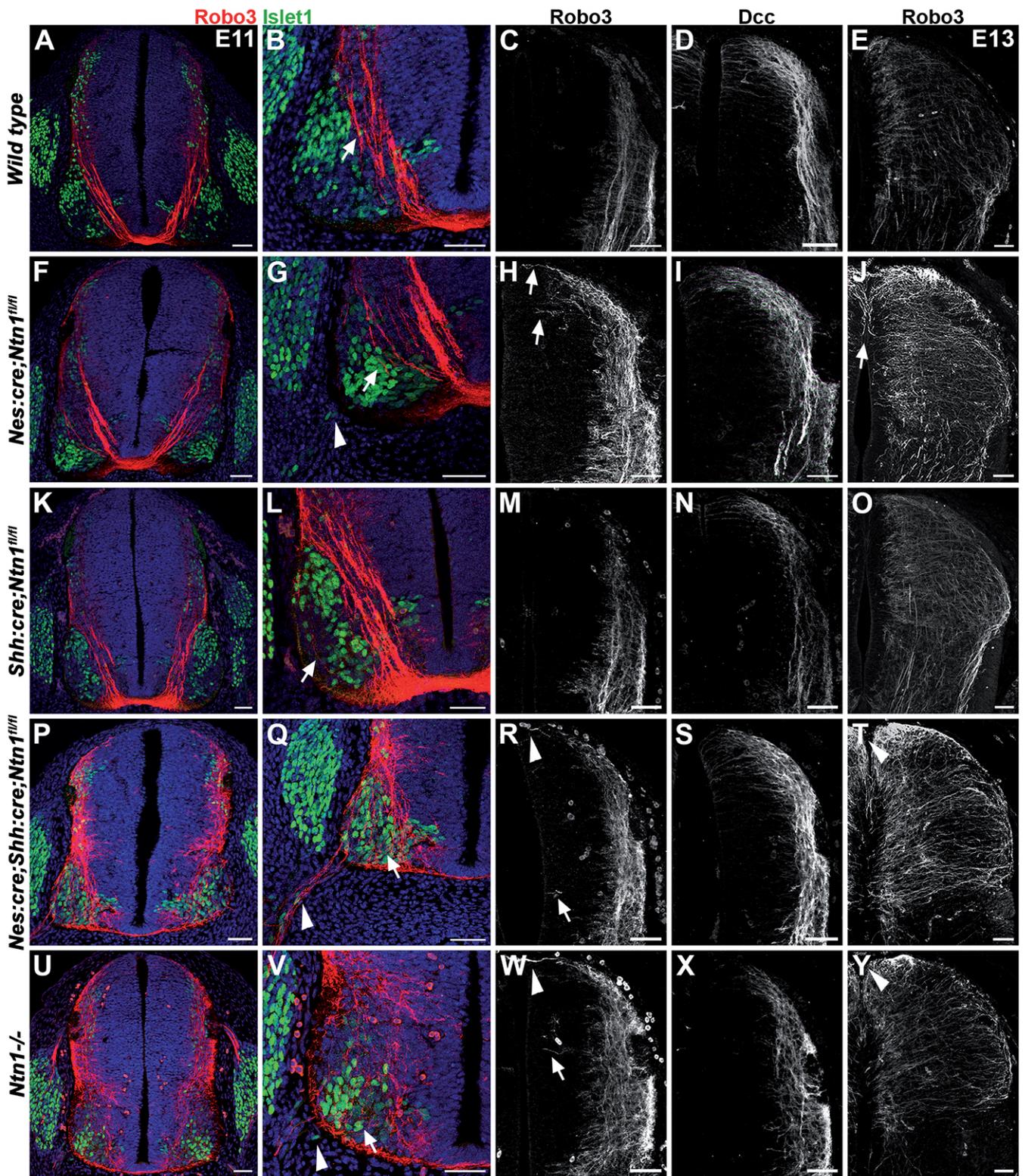
Figure S2 (Related to **Figure 1, Figure 2** and **Figure 4**)

Dorso-ventral commissural defects displayed by the different netrin1 mutant embryos.

Coronal cryostat sections of the brachial spinal cord at E11 and E13, labelled with Robo3 and Islet1 (A, B, F, G, K, L, P, Q, U and V), at E11 Robo3 (C, H, M, R, W), Dcc (D, I, N, S, X) and at E13, stained with Robo3 (E, J, O, T and Y). In wild type (A, B) the main Robo3+ fascicles don't cross the Islet1+ motor column (arrow in B). (C-E) Dorsally, the commissural axons avoid the roof plate and the VZ at E11 (C, D) and E13 (E). (F-J) In E11 *Nes:cre;Ntn1fl/fl* mutants (F-I) some Robo3+ axons invade the motor column area (F, arrow in G) and more dorsally, some of them cross the roof plate (arrows in H) . Moreover, some Islet1+ motor neurons, exit the CNS (arrowhead in G). At E13 Robo3+ axons massively project dorsally (arrow in J). In *Shh:cre;Ntn1fl/fl* embryos, some commissural axons are seen in the motor column (K, arrow in L) but there is not any defect in dorsal regions neither at E11 (M, N) nor at E13 (O). (P-Y) In *Nes:cre;Shh:cre;Ntn1fl/fl* embryos (P-T) and *Ntn1-/-* (U-Y) there is massive invasion of the motor columns (P, arrow in Q and U, arrow in V). Besides, some Robo3+ axons leave the CNS, through the motor roots in the double mutant (P, Q) and the DRGs in the knockout (U). Some Islet1+ motor neurons were found migrating through the motor root (arrowhead in Q and V). Dorsally both mutants display axons crossing the dorsal midline (arrowhead in R, T, W and Y) and invading the ventricular zone at E11 (arrowhead in R, S, arrowhead in W and X) and E13 (T, Y).

Scale bars: 50 µm in all panels.

A Robo3+ commissure thickness at E11

B Dcc+ commissure thickness at E11

C Neurofilament + commissure thickness at E11

D Robo3+ commissure thickness at E13

E Dcc+ commissure thickness at E13

F Neurofilament + commissure thickness at E13

G Robo1+ post-commissural bundle area

H Area of Robo3+ commissural axons in the motor column

I Area of Robo3+ commissural axons in the motor column

Wild type
Nes:cre; Ntn1^fl/fl
Shh:cre; Ntn1^fl/fl
Nes:cre; Shh:cre; Ntn1^fl/fl
Ntn1^-/-

6

Figure S3 (Related to **Figure 1, Figure 2** and **Figure 4**)

Quantifications of the ventral commissure thickness, post-commissural axon area and motor column invasion.

(A-F) The graphs represent the thickness of the commissure with different markers at E11 (A, B and C) and at E13 (D, E and F). (A) No reduction of ventral crossing is observed with Robo3 in *Nes:cre;Ntn1^{fl/fl}* mutants compared to controls. By contrast, a significant reduction is found between *wild type*, *Shh:cre;Ntn1^{fl/fl}*, *Nes:cre;Shh:cre;Ntn1^{fl/fl}* and *Ntn1^{-/-}* (-25%, -70% and -80% respectively). (B and C) This reduction was also seen with Dcc and Neurofilament labelling (-20%, -65% and -75%). Again, no difference was observed in *Nes:cre;Ntn1^{fl/fl}* mutants. (D, F) At E13, the thickness of the ventral commissure labelled with Robo3 or Neurofilament was similar between wild type and *Nes:cre;Ntn1^{fl/fl}* or *Shh:cre;Ntn1^{fl/fl}* mutants. However, it was still strongly reduced in *Nes:cre;Shh:cre;Ntn1^{fl/fl}* and *Ntn1^{-/-}* mutants (65% and 75% respectively). (E) Dcc labelling did not show any difference, except for *Nes:cre;Ntn1^{fl/fl}* mutants (15% reduction compared to *wild type*).

(G) Quantification of post-crossing axon surface. The graph represents the average size of the Robo1+ area next to the floor plate. There is no significant difference of the area occupied by post-commissural axons between *wild type* embryos and *Nes:cre;Ntn1^{fl/fl}* or *Shh:cre;Ntn1^{fl/fl}* mutants. This area is strongly reduced in *Nes:cre;Shh:cre;Ntn1^{fl/fl}* and *Ntn1^{-/-}* mutants (55% and 60% respectively), illustrating the reduction of midline crossing.

(H, I) Quantification of the invasion of the motor columns by Robo3+ commissural axons. The graph represents the area of the spinal cord motor column occupied by Robo3+ axons. In *Nes:cre;Ntn1^{fl/fl}* and *Shh:cre;Ntn1^{fl/fl}* embryos (H), there is a significant increase of Robo3 axons entering the motor columns. This increase is much higher (20 times more than in controls) in *Nes:cre;Shh:cre;Ntn1^{fl/fl}* and *Ntn1^{-/-}* mutants (I).

Data are represented as mean values ± SD. Results are considered non-significant (ns) for p-value > 0.05. Four levels of significance are represented: (*) when p-value < 0.05, (**) when p-value < 0.01, (***) when p-value < 0.001 and (****) when p-value < 0.0001. The dots on each graph represent the sections quantified for each genotype. 5 different sections were taken at the brachial level from at least 5 different embryos from 3 different litters.